Istraživanja i projektovanja za privredu
ISSN 1451-4117
DOI:10.5937/jaes0-53742
www.engineeringscience.rs

iipp publishing

Journal of Applied Engineering Science
Vol. 23, No. 1, 2025
Original Scientific Paper
Paper number: 23(2025)1, 1255, 90-98

EXPERIMENTAL ASSESSMENT OF FLEXURAL PERFORMANCE IN CONCRETE BEAMS REINFORCED WITH ANGLE STEEL PROFILES: A COMPARATIVE STUDY AGAINST TYPICAL REINFORCEMENT SYSTEMS

Ade Yuniati Pratiwi*, Hari Afriyono, Nursiah Chairunnisa, Wiku Adhiwicaksana Krasna, Ratni Nurwidayati, Ahmad Fahreza

Universitas Lambung Mangkurat, Engineering Faculty, Civil Engineering Study Program, South Kalimantan, Indonesia

** ade.pratiwi@ulm.ac.id*

This study investigates the performance of modified reinforced concrete (RC) beams with truss systems, specifically Pratt-truss and Warren-truss, compared to typical reinforcement systems through flexural strength tests. Aiming to enhance load-carrying capacity, the use of angle steel profiles in the truss systems to transform standard reinforcement bars was analyzed. The flexural strength evaluation involved eight specimens: two with conventional reinforcement, three with Pratt-truss, and three with Warren-truss, each measuring 15 x 15 x 120 cm. The focus was on initial stiffness, secant stiffness, and ductility. Results showed a notable performance increase with truss systems: a 7.5% rise in average initial stiffness, a 1.2% improvement in secant stiffness, and a 5.7% enhancement in displacement ductility, highlighting their potential for safer and more durable structures. The Pratt truss system exhibited the highest ductility, followed by the Warren truss and the standard system. Experimental observations indicated that the typical reinforcement system initially showed flexural cracks at the bottom of the beam, later followed by diagonal shear cracks, which intensified under load, causing concrete to crush in the compression zone. A similar pattern was observed in truss-reinforced beams, with initial flexural cracks at the beam's bottom progressing under load, ultimately resulting in concrete crushing in the same area. Crack propagation in both systems involved the formation and expansion of cracks along the diagonal and vertical framework, indicating flexural cracks.

Keywords: angle steel profile, pratt-truss, warren-truss, initial stiffness, secant stiffness, ductility, crack pattern

1 INTRODUCTION

Numerous methods to improve the flexural capacity and shear behavior of reinforced concrete beams have been studied over the past few decades, including the use of prestressed concrete and high-strength concrete [1], fiber-reinforced polymer (FRP) [2]–[7], steel fiber concrete [8,9], high-strength steel [10], and other types of reinforcement such as engineered cementitious composite combined with steel plates and hybrid steel bars in the reinforced concrete [11,12]. However, these solutions often require specialized materials and sophisticated construction technologies. Inadequate longitudinal reinforcement in concrete components makes them susceptible to flexural failure during specific loadings, such as earthquakes. Another technique for enhancing the flexural strength of concrete-reinforced beams is to apply steel trusses embedded in cast-in-place concrete beams [13,14]. A numerical study was conducted using steel trusses as the reinforcement system. The steel trusses, claimed to be more advantageous compared to rebar reinforcement, can bear the construction loads and serve as self-supporting elements during the construction phase. [15], However, experimental studies still needed to be done to understand and validate these claims. Recently, interest in this technology has been increasing, primarily due to the benefits it offers over standard reinforced concrete beams. Composite steel-concrete beams are frequently used for large-span beams with a low cross-sectional height in seismic-resistant framed constructions. The hybrid steel trussed concrete beam (HSTCB) is a common structural type in Italy, as it is a valuable instrument for light industrialization [16]–[18].

Another variation of reinforced concrete beams utilizing a steel truss system is presented by Tesser et al. [17]. This experimental study features a prefabricated concrete bottom flange, employing conventional rebar reinforcement for both the bottom and top, which function as the bottom and top chords of the truss, respectively. Additionally, the inclined bars are utilized as transverse reinforcement. The variables in the experimental tests were the various web reinforcements and depths. The results show the theoretical evaluations, and the flexural test results demonstrate that the flexural strength of hybrid truss beams is appropriately valued in Eurocode 2 [19] and Eurocode 4 [20]. Moreover, Quarantana et al. [21] illustrated the mechanical models and verification guidelines that must be applied while constructing these specific reinforced concrete beams to withstand static loads. Trentadue et al. [18] developed an analytical method to calculate the lateral-torsional buckling resistance moment in special truss-reinforced composite steel–concrete beams by estimating the critical elastic moment. Zhang et al. [13] conducted theoretical and experimental research to examine how embedded steel trusses affect the performance of reinforced concrete beams. Tests were conducted to determine the beams' ultimate shear capacity and structural performance with small shear span-to-depth ratios. The findings indicate that the best configuration for an embedded steel truss to enhance an RC beam's shear performance is an embedded steel angle truss with additional horizontal reinforcement. The experimental results also demonstrate that the structural performance of reinforced concrete beams in shear failure

would improve by embedding steel trusses within the beams. Most previous studies focused on changing the traditional reinforcement, and the trussed beams approach improves the flexural and shear behaviors of reinforced concrete beams. This paper's main objective is to investigate the flexural behavior of the steel truss systems, specifically Warren-truss and Pratt-truss, in reinforced concrete beams. Steel angles replaced the bottom and top longitudinal reinforcement to achieve a strength comparable to the conventional system. The flexural behavior, including initial stiffness, secant stiffness, ultimate load capacity, ductility, and crack pattern, was investigated using a two-point flexural loading test for the tested beams. The significance of this research is to offer insight into alternative reinforcement systems. Moreover, the design of the steel truss system has also been proposed using tensile strength equivalency for both longitudinal and transverse reinforcements.

2 MATERIALS AND METHODS

This study utilizes two concrete reinforcement systems: beams with typical reinforcement (rebar) and beams with a steel truss system. Beams with a truss system are divided into two types: Warren-truss and Pratt-truss. The difference between these two types lies in the arrangement of the truss.

2.1 Materials

There are three reinforcement systems, as shown in Fig. 1(a) and 1(b): typical reinforcement with rebar, Pratt-truss model, and Warren-truss model with angle steel profiles. The section view and cross-section of the reinforcement system are shown in Fig. 1(c) and (d), where the angle steel profile is assembled using welded connections, with the top serving as compression reinforcement and the bottom as tension reinforcement. The Pratt-truss and Warren-truss models using angle steel profiles are designed by converting a typical reinforcing bar into a simple beam. The tensile strength of the rebar is equivalent to the tensile strength of the angle steel profile at the same position in compression or tension. The tensile strength equivalency is shown in Eq. (1).

$$f_{yr}\, x\, A_r = f_{ya}\, x\, A_a \tag{1}$$

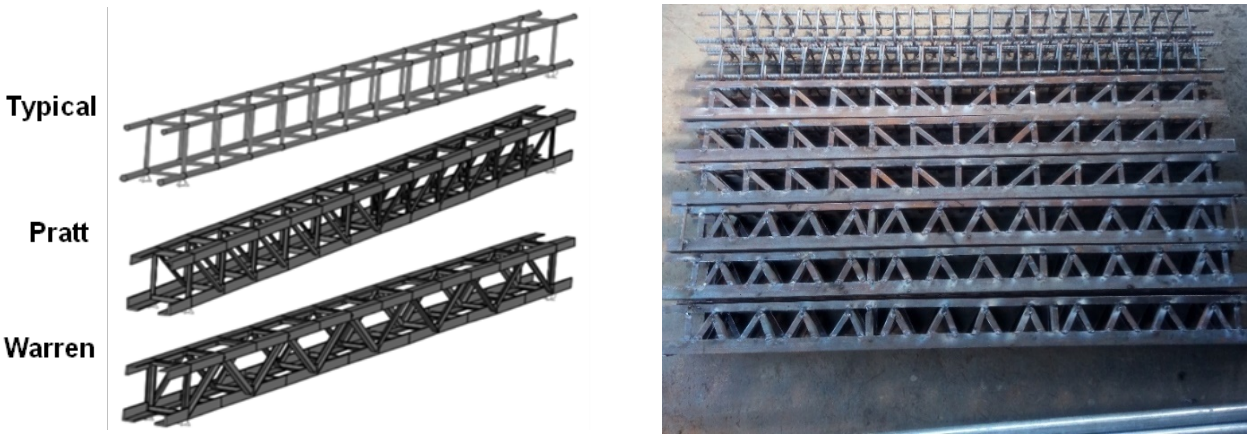

(a) Illustration of reinforcement systems

(b) Rebar, Pratt-truss, and Warren-truss models

(c) Section view of reinforcement system

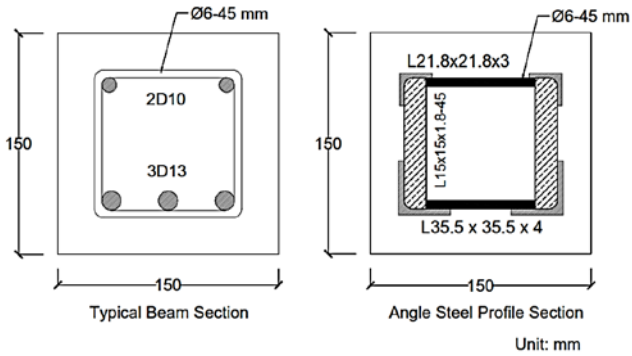

(d) Cross-section illustration

Fig. 1. The reinforcement systems and cross-section illustrations

Where f_{yr} is the rebar's yield strength, A_r is the rebar's total area at the top or bottom position, f_{ya} is the yield strength of the angle steel profile, and A_a is the total area of the angle steel profile needed at the top or bottom position. The details of the specimen and concrete compressive strength are shown in Table 1, while the steel properties of the reinforcement system are presented in Table 2. All specimens use a designed concrete compressive strength, f_c', 27

MPa and come from a concrete ready-mix plant. For steel properties, the rebar dimensions utilize a deformed bar for the primary or longitudinal bar and a plain bar for the transversal bar with a spacing of 45 mm. This arrangement is designed to capture a simple beam with a small span length. Transverse reinforcement in beams with angled steel profiles is determined by comparing it to the area of standard concrete transverse reinforcement as shown in Eq. (1). This equivalent area serves as a reference for calculating the necessity and size of the angled steel profiles used as transverse reinforcement. The transverse reinforcement area is calculated based on Eq. (2).

$$A_v = n \times \frac{1}{4}\pi D^2 \tag{2}$$

Where A_v is the area of transverse reinforcement, n is the number of transverse reinforcement legs, D is the diameter of transverse reinforcement.

Table 1. The detail of designed specimens

Beam Specimens	Reinforcement system	28 days concrete compressive strength, f_c'	Specimen details	Number of specimens
BT	Typical using rebar	29.70	Section size = 150 x 150 mm Length = 1200 mm Cover concrete = 25 mm	2
BP	Pratt-truss using angle steel profile	29.40		3
BW	Warren-truss using angle steel profile	28.65		3

Table 2. Steel properties for reinforcement system

Properties	Typical Reinforcing Bar (Rebar)		Angle Steel Profile	
	Longitudinal	Transversal	Longitudinal	Transversal
Yield strength (f_y)	390 MPa	235 MPa	285 MPa (bottom) 245 MPa (top)	245 MPa
Ultimate strength (f_u)	560 MPa	380 MPa	490 MPa (bottom) 400 MPa (top)	400 MPa
Dimension	3D13, mm (bottom) 2D10, mm (top)	Ø6–45 mm	2L 35.5 x 35.5 x 4 (bottom) 2L21.8x21.8x3 (top)	L15 x15 x1.8–45 mm (truss/diagonal) Ø6–45 mm (top and bottom)
Area	398 mm^2 (bottom) 157 mm^2 (top)	56.52 mm^2	544.62 mm^2 (bottom) 249.92 mm^2 (top)	54.21 mm^2
Modulus of Elasticity (E)	200.000 MPa			
Steel ratio, ρ	2.4% (bottom) 0.9% (top)		3.2% (bottom) 1.2% (top)	

2.2 Methods

This research employed a flexural strength test machine to examine the flexural strength of all specimens. The test specimens were positioned on a loading frame with joint support, and loading was conducted using a two-point load at one-third of the 36 cm span, following ASTM C78/C78M guidelines [22]. The load was applied using a hydraulic system, with load increments of 50 kg. The data obtained from the flexural strength test includes a load-displacement diagram and crack pattern. After obtaining the load-displacement values, they were plotted on the diagram, and the crack, yield, and ultimate points were determined based on strain gauge readings and observations during the experiment. These points are crucial for obtaining the initial stiffness, secant stiffness, and beam ductility. Crack patterns were also observed because they are essential for understanding the behavior and type of failure in the beam, whether flexural or shear. The test setup is shown in Fig. 2.

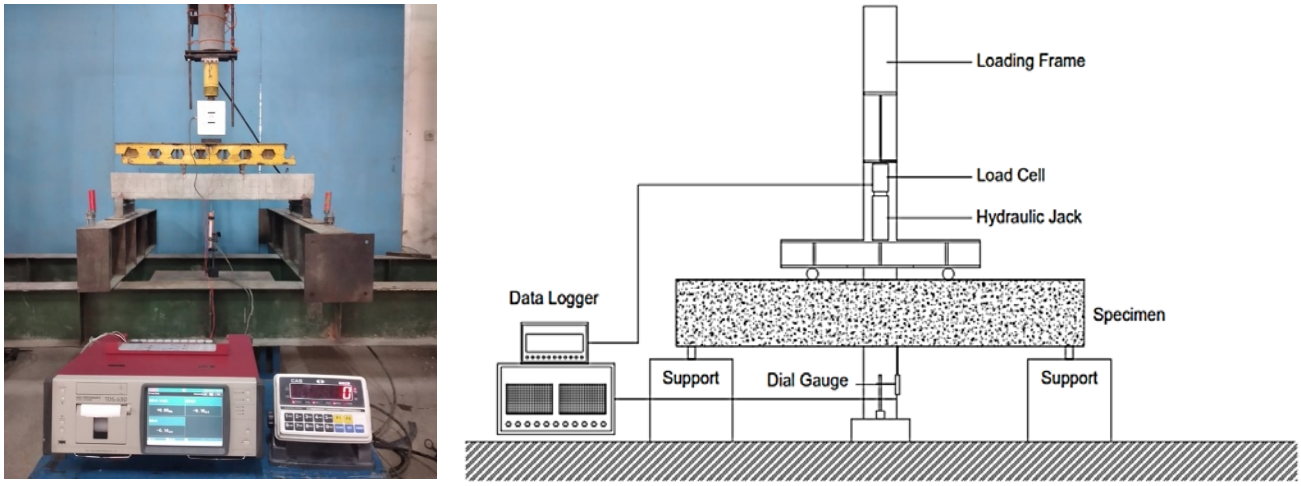

Fig. 2. The flexural strength test setup

3 RESULTS AND DISCUSSION

3.1 Flexural Strength Test Results

Flexural strength testing provides insights into the relationship between load and displacement, as presented in Fig. 3. The flexural strength test results determine the crack, yield, and ultimate values. The crack point is based on the visual observation of the first crack. The crack point is related to the first crack load and crack displacement, the yield point is obtained from the first yielding of the rebar or angle steel profile, which is related to the yielding load and yielding displacement, and lastly, the ultimate point is determined from a point before the sudden decrease in strain gauge readings, which is related to the ultimate load and ultimate displacement point. The load–displacement relationship determines initial stiffness, secant stiffness, and ductility values. Initial stiffness or elastic stiffness indicates the initial resistance of an element—the higher the initial stiffness, the greater the initial resistance of the element. This concept is crucial in the design phase, as it helps engineers understand how much load a structure can initially bear. Initial stiffness is calculated based on the tangential value or slope from the zero point to the yield point. Secant stiffness, conversely, is the effective stiffness calculated based on the slope of the line drawn from the zero point to the ultimate point. This value is essential in understanding how much energy a structure can dissipate before failure. Additionally, the ductility value is the ratio between ultimate and yield displacement. Ductility is an essential indicator of the plastic work of an element under load and requires both yielding and plastic behavior, which is crucial in predicting how a structure will behave under extreme conditions. The results of determining the crack point, yield, ultimate, initial stiffness, secant stiffness, and ductility can be seen in Table 3.

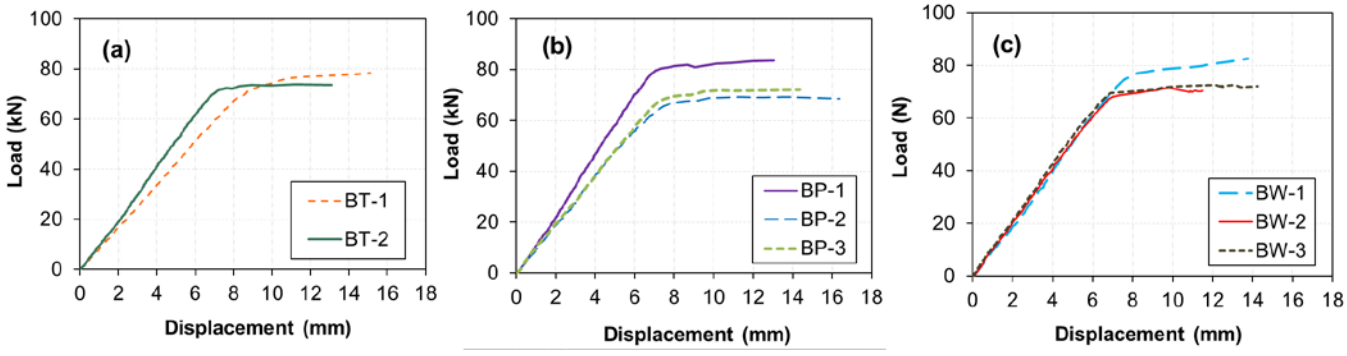

Fig. 3. The load-displacement curve based on flexural strength test results for (a) Typical reinforcement system, (b) Pratt-truss reinforcement system, and (c) Warren-truss reinforcement system

Table 3. Flexural strength test results

Specimen	V_{cr} (kN)	Δ_{cr} (mm)	V_y (kN)	Δ_y (mm)	V_u (kN)	Δ_u (mm)	$K_i = \frac{V_y}{\Delta_y}$ (kN/mm)	$K_e = \frac{V_u}{\Delta_u}$ (kN/mm)	$\mu_\Delta = \frac{\Delta_u}{\Delta_y}$
BT-1	22.06	2.66	68.65	8.18	78.45	15.12	8.39	5.19	1.85
BT-2	19.61	2.06	71.10	7.12	73.58	13.12	9.99	5.61	1.84
BP-1	32.36	2.84	79.43	7.04	83.65	13.06	11.28	6.41	1.86

Specimen	V_{cr} (kN)	Δ_{cr} (mm)	V_y (kN)	Δ_y (mm)	V_u (kN)	Δ_u (mm)	$K_i = \frac{V_y}{\Delta_y}$ (kN/mm)	$K_e = \frac{V_u}{\Delta_u}$ (kN/mm)	$\mu_\Delta = \frac{\Delta_u}{\Delta_y}$
BP-2	24.52	2.68	66.69	7.76	68.45	16.38	8.59	4.18	2.11
BP-3	34.81	3.66	67.67	7.22	72.26	14.36	9.37	5.03	1.99
BW-1	20.59	2.26	74.04	7.5	82.72	13.78	9.87	6.00	1.84
BW-2	28.93	2.84	66.19	6.68	70.34	11.48	9.91	6.13	1.72
BW-3	22.06	2.08	67.18	6.54	72.08	14.26	10.27	5.05	2.18

Where V_{cr} is the cracking load, Δ_{cr} is displacement at cracking, V_y is the yielding load, Δ_y is displacement at yielding, V_u is the ultimate load, Δ_u is displacement at the ultimate point, K_i is initial stiffness, K_e is secant stiffness, and μ_Δ is ductility based on displacement [23]. Based on Fig. 3 (b), the load-displacement results for BP show similar values, except for BP-1. A similar behavior is also shown in Fig. 3 (c) for BW-1. To identify whether BP-1 and BW-1 are outliers, Grubb's test is employed [24], which is a method to detect outliers from normally distributed data. Grubb's test uses sample values of V_u for BP and BW. Both BP-1 and BW-1 were found to be the farthest from the data set but were not classified as outliers since none of the Grubb's values exceed Grubb's Critical. Grubb's values for BP-1 and BW-1 were 1.12 and 1.14, while the Grubb's Critical was 1.15 with a significance level of 0.05. Therefore, it is acceptable to use all data for further analysis. The analysis of Grubb's test is presented in Table 4. For specimens BT-1 and BT-2, Grubb's test cannot be performed because a minimum of three data points is required. The critical values for Grubb's test are obtained from Grubb's critical value table.

Table 4. Grubb's test analysis

Specimen	V_u (kN)	Mean Value (kN)	Standard Deviation	Grubb's Value	Grubb's Critical for $\alpha = 0.05$	Outlier
	X_i	$\bar{X}$	$S_D = \sqrt{\frac{(X_i - \bar{X})^2}{n-1}}$	$G_i = \frac{\lvert X_i - \bar{X} \rvert}{S_D}$	$G_{critical}$	$G_i > G_{critical}$
BT-1	78.45	76.02	3.44	0.71	Not Available	-
BT-2	73.58			0.71	Not Available	-
BP-1	83.65	74.79	7.91	1.12	1.15	No
BP-2	68.45			0.80	1.15	No
BP-3	72.26			0.32	1.15	No
BW-1	82.72	75.05	6.70	1.14	1.15	No
BW-2	70.34			0.70	1.15	No
BW-3	72.08			0.44	1.15	No

Generally, an increase in initial resistance is observed for the truss reinforcement system. Moreover, based on Fig. 4, the average results of the initial stiffness values indicate that modifying the typical reinforcement system into a truss system increases the initial stiffness by 7.5%. The truss system shows a higher, albeit not significant, increase of 1.2% for secant stiffness. As for the ductility value, the truss system also increased by an average of 5.7%. Based on the load-displacement values, the differences between the three models are not significant, with V_u values of 76.02, 74.79, and 75.05 kN for BT, BP, and BW, respectively.

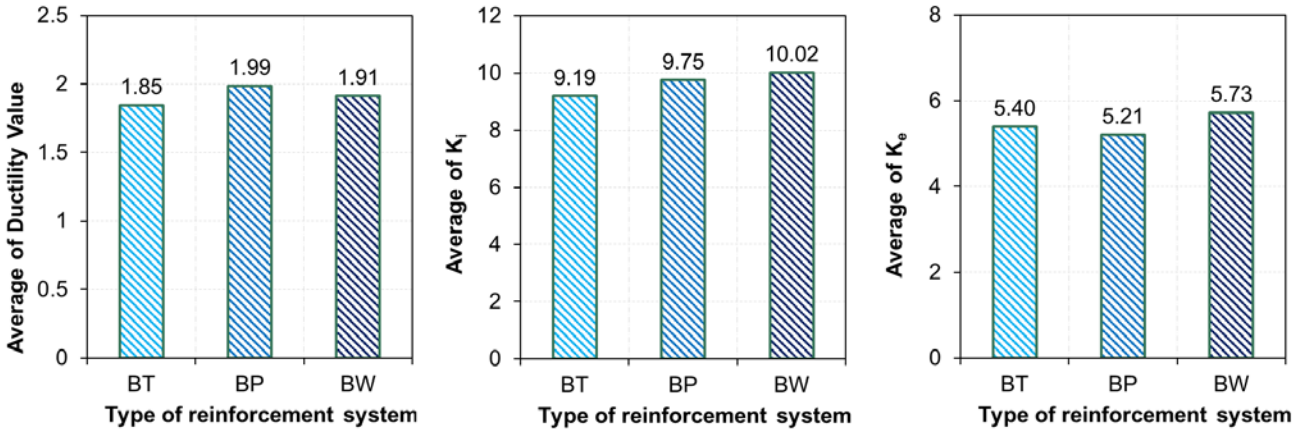

Fig. 4. The average values of (a) ductility, (b) initial stiffness, and (c) secant stiffness

Based on the load-displacement curve, it is also desirable to evaluate the ductility based on energy under the curve. The energy-based ductility index utilizes energy to evaluate ductility and apply the observation to structures experiencing earthquake loads; it can also be applied to static load conditions [25],[26]. These indexes compare a structural member's total ultimate energy against its service-level energy, as detailed in Eq. (2) [5]. The total area under its load-displacement curve depicts the overall energy a member holds. Similarly, the energy at the service level is indicated by the area under the curve up to the service load point [4],[25],[27]. Naaman and Jeong [3] use another approach to calculate ductility based on energy, which is shown in Eq. (3).

$$\mu_E = \frac{E_{total}}{E_{ys}} \tag{2}$$

$$\mu_E = 0.5\left(\frac{E_{total}}{E_{el}} + 1\right) \tag{3}$$

Where μ_E is the ductility based on energy under the curve, E_{total} is the total area under the curve, E_{ys} is the total area under the yielding point, or service area, and E_{el} is similar to E_{ys}, which are defined as the area under the elastic stage.

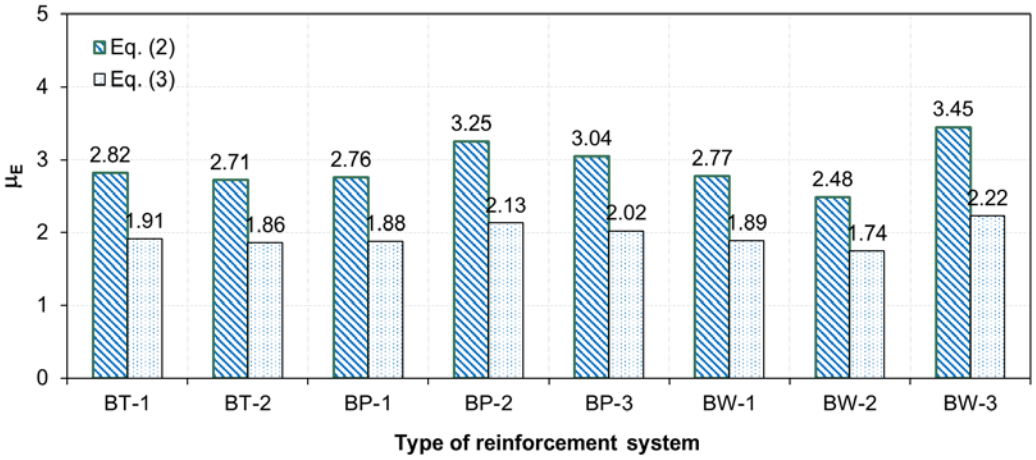

Fig. 5. Energy-based ductility index of the typical and truss reinforcement system

Ductility, as illustrated in Fig. 5, is evaluated based on the energy under the curve. There are differences in the results when using the methods by Naaman and Jeong [3] in Eq. (3) compared to those by Thomsen et al. [5] in Eq. (2). The method in Eq. (3) yields lower results, as it was initially developed to analyze the behavior of reinforced concrete beams under cyclic loading. However, it can also be used for monotonic loads, as the backbone curve in cyclic loading exhibits similar behavior to monotonic loads. When comparing a typical reinforcement system with a truss system, the ductility index based on the area under the curve aligns with the displacement-based ductility results shown in Fig. 4(c). Generally, BT specimens exhibit lower results, followed by BW, with the highest results observed in BP. Based on the results, it can be concluded that the RC beam with a truss reinforcement system exhibits higher flexural capacity, which aligns with the research by Prahallada et al. [28].

3.1.1 Crack pattern

The crack pattern for the typical reinforcement system BT-1 and BT-2 can be seen in Fig. 6. The crack pattern for the Pratt-truss reinforcement system, namely BP-1, BP-2, and BP-3, can be seen in Fig. 7, while the Warren-truss

reinforcement system can be seen in Fig. 8. Crack patterns in BT-1 and BT-2 differ from those in specimens BP-1, BP-2, BP-3, BW-1, BW-2, and BW-3. In specimens BT-1 and BT-2, the first crack occurs vertically at the bottom of the beam in the middle of the span, namely in the tensile area, and then rises towards the compressive section with increasing load until concrete crushing occurs. This crack is referred to as a flexural crack. Additionally, inclined diagonal cracking occurs from the shear spans towards the load point. Diagonal cracking indicates that the combination of flexural and shear cracking can be caused by increased load, resulting in reduced aggregate interlocking [29].

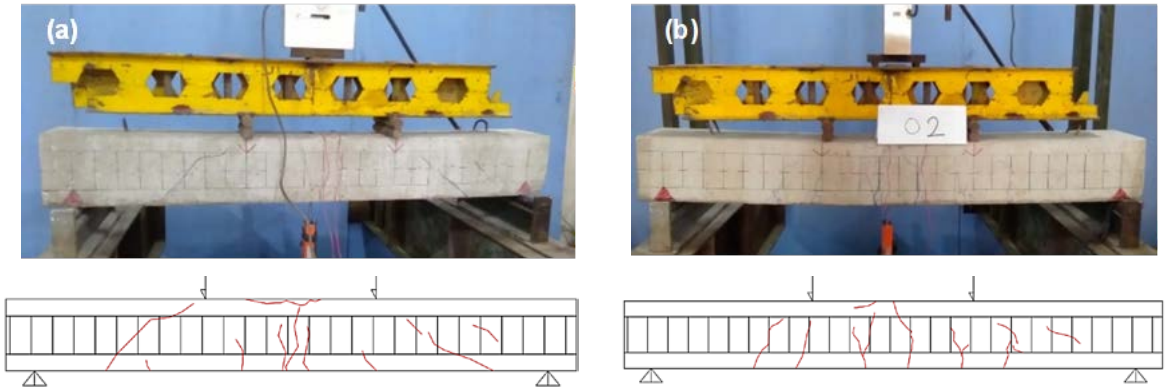

Fig. 6. Crack pattern of Typical reinforcement system for: (a) BT-1 and (b) BT-2

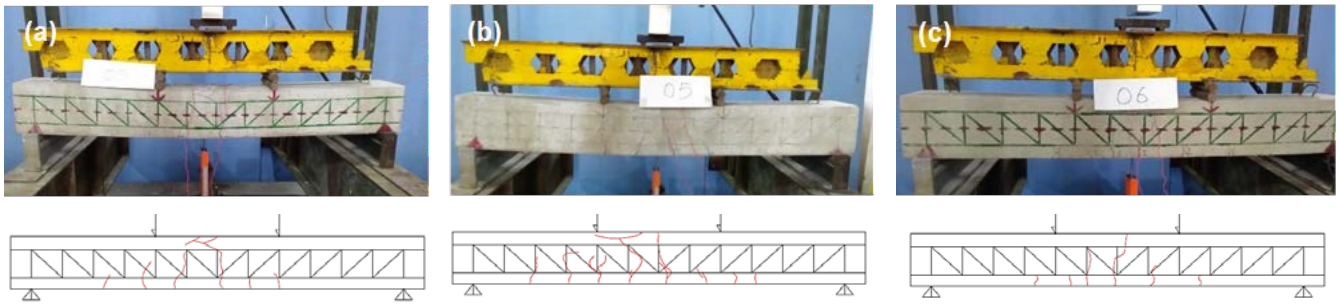

Fig. 7. Crack pattern of Pratt-truss reinforcement system for (a) BP-1, (b) BP-2, and (c) BP-3

Vertical cracks in beams BP-1, BP-2, and BP-3 occurred more at the center of the span. The first cracks originated from the bottom of the beam or tensile area and increased towards the top of the concrete or compressive area as the load acting on the beam increased. These are called flexural cracks, indicating the occurrence of flexural collapse in the beam. Cracks occur following the arrangement of the vertical and diagonal trusses. Similar to the Pratt-truss reinforcement system, the cracks in BW-1, BW-2, and BW-3, as seen in Fig. 8, were concentrated in the mid-span area. The first flexural cracking occurred from the bottom of the beam or tensile area. Then, with increasing load, the crack propagated through the angle steel profile and increased towards the top of the concrete or compressive area until crushing occurred. The pure bending failure may be due to the triangular shape of the steel truss system. The triangulated geometry of the steel truss system can engage in a truss-like action that redistributes shear stresses, reducing reliance on traditional shear reinforcements like stirrups. However, this behavior also highlights the limitations of Eq. (1) for transverse reinforcement, as it does not consider the inclination of steel profiles for BW and BP specimens, indicating the need for a more comprehensive solution.

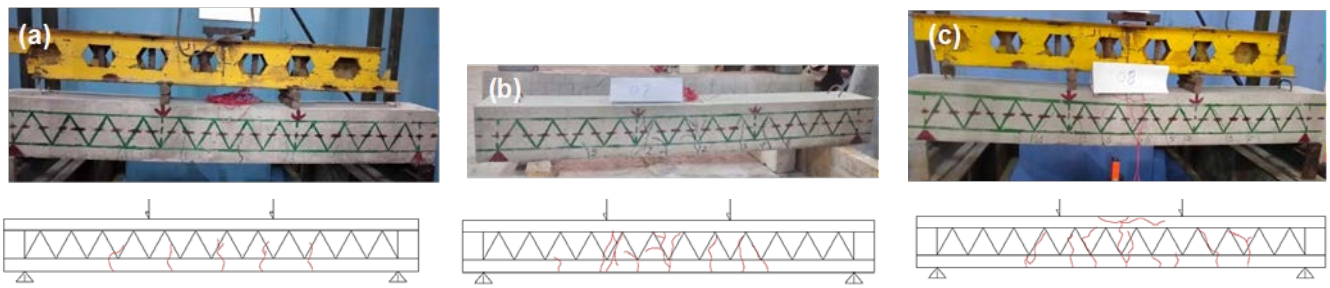

Fig. 8. Crack pattern of the Warren-truss reinforcement system for (a) BW-1, (b) BW-2, and (c) BW-3

3.1.2 Design recommendations

Below are proposed design recommendations for the steel truss system embedded in concrete:

1. It is recommended to use angle profiles for longitudinal and transverse reinforcements and Pratt truss for the steel truss configuration. The stirrups in typical reinforcement should be replaced by triangular or diagonal steel. It is also recommended to increase the steel ratio in the bottom chord to enhance the vertical load-bearing capacity.
2. The design capacity of beams using the steel truss system should be calculated and adjusted based on the ACI 318 code for typical reinforced concrete.
3. It is recommended to use tensile strength equivalency as shown in Eq. (1) for the longitudinal reinforcement design. First, design the reinforced concrete beam using a typical reinforced beam. Second, when the designed reinforcement is achieved for both the bottom and top chords of the beam, use tensile strength equivalency for each chord to determine the area of the steel profile.
4. Eq. (1) has a limitation in that it will only apply to longitudinal reinforcement as it cannot capture the inclined steel profile contribution. The design procedure for transverse reinforcement should use the shear reinforcement formula as shown in ACI 318-19 at equation 22.5.8.5.4 or in Eurocode 2 at equations 6.13 and 6.14.

4 CONCLUSIONS

Based on the findings and discussions presented in the preceding sections, the following conclusions have been drawn:

1. Modifying the typical reinforcement system using a truss system, namely Pratt and Warren, in reinforced concrete beams can lead to a 7.5% increase in the average initial stiffness, a 1.2% increase in the secant stiffness, and a 5.7% improvement in the displacement ductility. These results underscore the potential of truss systems in enhancing the performance of reinforced concrete beams.
2. Based on the ductility calculated by reviewing the energy produced, the Pratt truss system exhibits the highest ductility, followed by the Warren truss and the typical reinforcement system.
3. The typical reinforcement system displays initial cracking in the form of flexural cracks at the bottom of the beam, which intensifies with increasing load until diagonal shear cracks appear, ultimately leading to concrete crushing in the compression zone. Similarly, the truss reinforcement system exhibits a comparable crack pattern, with initial flexural cracks at the bottom of the beam that escalate as the load increases, culminating in concrete crushing in the compression zone. Crack propagation, the process of crack formation and expansion, occurs along the entire length of the diagonal and vertical framework, resulting in flexural cracks.

5 ACKNOWLEDGEMENT

The authors gratefully acknowledge the financial support received from the BIMA Research Grant Program under contract number 056/E5/PG.02.00.PL/2024 and derivative contract number 1064/UN8.2/PG/2024, funded by the Ministry of Research, Technology and Higher Education of the Republic of Indonesia through LPPM ULM.

6 REFERENCES

[1] Hao, N., Yang, Y., Xue, Y., Feng, S., Yu, Y., Wang, C., and Li, Y. (2023). Experimental study on flexural behavior of partially precast high-strength steel reinforced ultra-high performance concrete beam. Engineering Structures. vol. 284, DOI: 10.1016/j.engstruct.2023.115999.

[2] Jeong, S. M. and Naaman, A. E. (1995). Ductility of concrete beams prestressed with FRP tendons, in Structures Congress - Proceedings, 1995, vol. 2.

[3] Naaman, A. E. and Jeong, S. M. (1995). Structural ductility of concrete beams prestressed with FRP tendons, 1995.

[4] ACI 440.1R-15 (2015). Guide for the design and construction of structural concrete reinforced with fiber-reinforced polymer FRP bars. American Concrete Institute, 2015.

[5] Thomsen, H., Spacone, E., Suchart L., and Camata, G. (2004). Failure mode analyses of reinforced concrete beams strengthened in flexure with externally bonded fiber-reinforced polymers. Journal of Composites for Construction. DOI: 10.1061/(ASCE)1090-0268(2004)8:2(123).

[6] Khan, A. Q., Pimanmas, A., and Chindaprasirt, P. (2023). Flexural strengthening of RC beams using Sisal Fibre Reinforced Polymer (SFRP) composite with anchorage systems. Results in Engineering. vol. 18, DOI: 10.1016/j.rineng.2023.101116.

[7] Raoof, S. M., Koutas, L. N., and Bournas, D. A. (2017). Textile-reinforced mortar (trm) versus fibre-reinforced polymers (FRP) in flexural strengthening of RC beams. Construction and Building Materials. vol. 151, DOI: 10.1016/j.conbuildmat.2017.05.023.

[8] Kavya Sameera, V. and Keshav, L. (2022). Properties and performance of steel fiber reinforced concrete beam structure – review. Materials Today: Proceedings. vol. 66. pp. 916–919, DOI: 10.1016/j.matpr.2022.04.643.

[9] Wang, L., Song, Z., Huang, C., Ma, L., and Fu, F. (2020). Flexural capacity of steel-FCB bar-reinforced coral concrete beams. Structural Concrete. vol. 21, no. 6, DOI: 10.1002/suco.201900409.

[10] Haryanto, Y., Han, A. L., Hu, H.-T., Hsiao, F.-P., Hidayat, B. A., and Widyaningrum, A. (2021). Enhancement of flexural performance of RC beams with steel wire rope by external strengthening technique. Journal of the Chinese Institute of Engineers. vol. 44, no. 3. pp. 193–203, DOI: 10.1080/02533839.2021.1871651.

[11] Liu, L., Yu, S., and Ma, X. (2023). Flexural capacity of RC beams reinforced with ECC layer and steel plate. Journal of Building Engineering. vol. 65, DOI: 10.1016/j.jobe.2022.105781.

[12] Wei, B., He, X., Zhou, M., Wang, H., and He, J. (2024). Experimental study on flexural behaviors of FRP and steel bars hybrid reinforced concrete beams. Case Studies in Construction Materials. vol. 20, DOI: 10.1016/j.cscm.2023.e02759.

[13] Zhang, N., Fu, C. C., Chen, L., and He, L. (2016). Experimental studies of reinforced concrete beams using embedded steel trusses. ACI Structural Journal. vol. 113, no. 4, DOI: 10.14359/51688616.

[14] Arafa, M., Alqedra, M. A., and Salim, R. (2018). Performance of RC beams with embedded steel trusses using nonlinear fem analysis. Advances in Civil Engineering. vol. 2018. pp. 1–8, DOI: 10.1155/2018/9079818.

[15] Wang, K., Zhu, Z., Luo, H., and Omar, A. A. (2021). Analysis on flexural capacity of square steel tube truss concrete beams with grouted chords. Advances in Materials Science and Engineering. vol. 2021, DOI: 10.1155/2021/6694291.

[16] Colajanni, P., La Mendola, L., and Recupero, A. (2013). Experimental test results vs. analytical prediction of welded joint strength in hybrid steel trussed concrete beams (HSTCBS). European Journal of Environmental and Civil Engineering. vol. 17, no. 8. pp. 742–759, DOI: 10.1080/19648189.2013.815135.

[17] Tesser, L. and Scotta, R. (2013). Flexural and shear capacity of composite steel truss and concrete beams with inferior precast concrete base. Engineering Structures. vol. 49. pp. 135–145, DOI: 10.1016/j.engstruct.2012.11.004.

[18] Trentadue, F., Quaranta, G., Carlo Marano, G., and Monti, G. (2011). Simplified lateral-torsional buckling analysis in special truss-reinforced composite steel-concrete beams. Journal of Structural Engineering. vol. 137, no. 12. pp. 1419–1427, DOI: 10.1061/(ASCE)ST.1943-541X.0000390.

[19] European Committee for Standardization (2005). Eurocode 2: design of concrete structures - part 1-1: general rules and rules for buildings, 2005.

[20] European Committee for Standardization (2004). Eurocode 4: design of composite steel and concrete structures-part 1-1: general rules and rules for buildings.

[21] Quaranta, G., Petrone, F., Marano, G. C., Trentadue, F., and Monti, G. (2010). Structural design of composite concrete-steel beams with spatial truss reinforcement elements. Asian Journal of Civil Engineering. vol. 12, no. 2. pp. 155–178.

[22] ASTM C78/C78M-22 (2022). Standard test method for flexural strength of concrete (using simple beam with third-point loading), United States.

[23] Park, R. and Paulay, T. (1975). Ultimate deformation and ductility of members with flexure, in Reinforced Concrete Structures, Wiley, 1975, pp. 195–269. DOI: 10.1002/9780470172834.ch6.

[24] Grubbs, F. E. (1950). Sample criteria for testing outlying observations. The Annals of Mathematical Statistics. vol. 21, no. 1. pp. 27–58, DOI: 10.1214/aoms/1177729885.

[25] Ling, J. H., Lim, Y. T., and Jusli, E. (2023). Methods to determine ductility of structural members: a review. Journal of the Civil Engineering Forum. pp. 181–194, DOI: 10.22146/jcef.6631.

[26] Hason, M. M., Hanoon, A. N., Saleem, S. J., Hejazi, F., and Al Zand, A. W. (2021). Characteristics of experimental ductility energy index of hybrid-CFRP reinforced concrete deep beams. SN Applied Sciences. vol. 3, no. 2, DOI: 10.1007/s42452-021-04202-6.

[27] Ghallab, A. (2014). Ductility of externally prestressed continuous concrete beams. KSCE Journal of Civil Engineering. vol. 18, no. 2. pp. 595–606, DOI: 10.1007/s12205-014-0443-0.

[28] Prahallada, M. C., Naveen Kumar, D. T., and Chandrashekhar, S. Y. (2018). Behaviour of pre-fabricated steel truss as reinforcement in RC beams. International Journal of Pure and Applied Mathematics. vol. 120, no. 6. pp. 6691–6708.

[29] Taylor, R. (1959). A note on the mechanism of diagonal cracking in reinforced concrete beams without shear reinforcement. Magazine of Concrete Research. Vol. 11. Pp.159-162. DOI: 10.1680/macr.1959.11.33.159

Paper submitted: 26.09.2024.

Paper accepted: 25.12.2024.